Evaluation of N-Aromatic Maleimides as Free Radical Photoinitiators: A Photophysical and Photopolymerization Characterization

Chris W. Miller,[†] E. Sonny Jönsson,[‡] Charles E. Hoyle,*[,†] Kalyanaraman Viswanathan,[†] and Edward J. Valente[§]

School of Polymers and High Performance Materials, The University of Southern Mississippi, Hattiesburg, Mississippi 39406, Fusion UV-Curing Systems, Gaithersburg, Maryland, and Department of Chemistry, Mississippi College, Clinton, Mississippi 39058

Received: August 2, 2000; In Final Form: November 27, 2000

Photopolymerizable compositions were prepared using acrylate monomers in combination with various N-aromatic maleimides. N-aromatic maleimides were segregated into two groups: those that could adopt a planar conformation and those that could not adopt a planar conformation. The maleimides were characterized using single-crystal X-ray diffraction spectroscopy, laser flash photolysis spectroscopy, UV−vis absorption spectroscopy, and photodifferential scanning calorimetry. Planar N-aromatic maleimides were found to have a low relative excited-state triplet yield, showing significant shift of the primary maleimide UV absorption band with changes in solvent polarity, and did not initiate free radial polymerization upon direct UV excitation. Twisted N-aromatic maleimides have a higher relative triplet yield, show negligible shift of the primary maleimide UV absorption band, with solvent polarity, and initiate free radical polymerization upon direct excitation. Addition of benzophenone was found to dramatically increase the initiation efficiency of both planar and twisted N-aromatic maleimides to levels approaching that of conventional cleavage photoinitiators.

Introduction

N-substituted maleimides have been known in organic and polymer chemistry for many years. Recently we have shown that N-aliphatic maleimides and N-alkylmaleimides (Figure 1) may be used as free radical photoinitiators of acrylate monomers.[1] N-aliphatic maleimides initiate free radical polymerization through a hydrogen atom abstraction process in the presence of hydrogen atom donors such as alcohols and ethers (Scheme 1). In the presence of hydrogen atom donors such as amines and vinyl ethers, radicals are produced through an electron-transfer/proton-transfer reaction sequence.[2,3] Both direct abstraction and electron/proton transfer result in the formation of two radicals capable of initiating polymerization: a succinimido radical on the maleimide residue, and a radical on the hydrogen atom donor. In comparison, conventional hydrogen atom abstraction type photoinitiators produce only a single initiating radical as a result of the hydrogen-transfer process. Real-time Fourier transform infrared spectroscopy and real-time UV−vis spectroscopy have shown that when N-aliphatic maleimides are used as photoinitiators in acrylic systems, essentially all of the maleimide chromophores are consumed in the polymerization process.[2,4] Three possible reactions may account for consumption of the maleimide chromophores: (1) initiation of polymer chains through hydrogen atom abstraction or electron/proton-transfer processes, (2) copolymerization with the acrylic monomers, and (3) maleimide [2+2] cycloaddition reactions.[5−11] At the low concentrations of maleimide used to initiate free radical acrylate polymerization, initiation and copolymerization reactions are the dominant pathways for maleimide consumption.

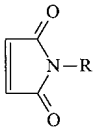

Figure 1. Structure of N-aliphatic maleimides and *N*-alkylmaleimides: R = alkyl or aliphatic group.

SCHEME 1. Proposed Initiation Mechanisms for *N*-Alkylmaleimides

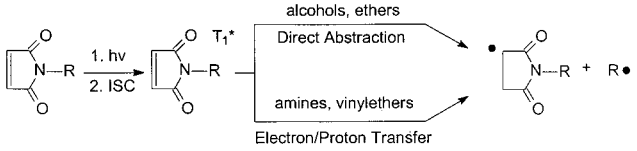

While N-aliphatic and N-alkylmaleimides have been shown to initiate free radical polymerization efficiently, they are typically difficult to synthesize in high purity and high yield. N-aromatic maleimides are much easier to synthesize. The objective of the present work was to synthesize a number of substituted N-aromatic maleimides and evaluate their utility as free radical photoinitiators for acrylic-based formulations. To this end, 16 N-aromatic maleimide (ARMI) and isomaleimide derivatives with various combinations of substituents were prepared (Figures 2 and 3) and evaluated. The small-molecule photochemical and photophysical properties of the N-aromatic maleimides were characterized using UV−vis absorption spectroscopy, laser flash photolysis transient absorption spectroscopy, and low-temperature emission spectroscopy. The relative photopolymerization efficiency of a difunctional acrylate when initiated by various N-aromatic maleimides was compared using photodifferential scanning calorimetry. Trends from the small-molecule studies and photopolymerizations were correlated with torsion angles between the phenyl ring and imide ring in the

* To whom correspondence should be addressed. Phone: (601) 266-4873. Fax: (601) 266-5504.
[†] The University of Southern Mississippi.
[‡] Fusion UV-Curing Systems.
[§] Mississippi College.

10.1021/jp002811v CCC: $20.00
Published on Web 03/21/2001

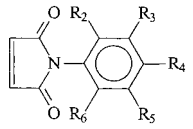

PMI - R_2,R_3,R_4,R_5,R_6 = H
2FPMI - R_3,R_4,R_5,R_6 = H; R_2 = F
2ClPMI - R_3,R_4,R_5,R_6 = H; R_2 = Cl
2BrPMI - R_3,R_4,R_5,R_6 = H; R_2 = Br
2IPMI - R_3,R_4,R_5,R_6 = H; R_2 = I
2tBPMI - R_3,R_4,R_5,R_6 = H; R_2 = t-butyl
2CF_3PMI - R_3,R_4,R_5,R_6 = H; R_2 = CF_3
4CF_3PMI - R_2,R_3,R_5,R_6 = H; R_4 = CF_3
2,6DIPPMI - R_3,R_4,R_5 = H; R_2, R_6 = isopropy
2Br35CF_3PMI - R_4 = H; R_2 = Br; R_3,R_5 = CF_3

Figure 2. N-aromatic maleimide general structure. Substituents were chosen from among those listed.

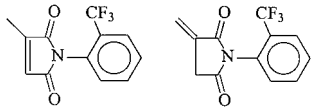

2CF3PCI 2CF3PII

Figure 3. Isomaleimide structures.

molecules calculated from single-crystal X-ray diffraction crystal structures. Photopolymerization of the difunctional monomer was also conducted for samples with maleimide, amine, and benzophenone present.

Experimental Section

1. Materials and Synthesis. *N*-Phenylmaleimide (PMI) and *N*-methylmaleimide (MMI) were obtained from Aldrich Chemical Co. and purified by recrystallization and/or sublimation. *N*-(4-Methylphenyl)maleimide (4CH3PMI), *N*-(4-methoxyphenyl)maleimide (4OCH3PMI), and *N*-(4-cyanophenyl)maleimide (4CNPMI) were prepared by standard procedures. All other ARMI derivatives were prepared using the general procedure given below and were purified by sublimation and/or recrystallization. 1,6-Hexanediol diacrylate (HDDA) was obtained from UCB Radcure and Aldrich and used as received. Poly(ethylene glycol)-400-diacrylate (PEG400DA) and all other reagents, solvents, and materials were obtained from and used as received unless otherwise specified.

A general synthesis: Maleic anhydride (typical ~33 g) was placed in diethyl ether (100 mL) and allowed to dissolve. The requisite aromatic amine (typically ~41 mL) was added squirtwise to the stirring solution. The reaction was allowed to proceed at room temperature overnight, and a pale white precipitate was observed. (Note: In cases where the aniline is unsubstituted or is substituted with an electron-donating substituent, it is necessary cool the anhydride solution in an ice bath during addition of the substituted aniline.) The stirring solution was then warmed for several hours and filtered, yielding a pale white solid. The mother liquor was then combined with the wash liquor and allowed to stir again, and additional product was filtered off. The solids were then combined and dried in a vacuum. Typical yields of the maleamic acid were 90−98%. The maleamic acid was then placed in a round-bottomed flask with 100 mL of toluene and 25 mL of DMSO, and allowed to dissolve. Concentrated sulfuric acid (1.8 mL) was then added to the stirring mixture, which was then heated to ~130 °C. The reaction mixture was allowed to reflux for 4 h or until an azeotrope was no longer observed in the Dean−Stark trap used to remove water from the reaction mixture. Excess toluene was removed via vacuum distillation. The mixture was then added to stirring distilled water to precipitate the imide and remove excess DMSO. The aqueous suspension was allowed to stir overnight and was filtered. The pale white solid thus obtained was dried under vacuum. Maleimide yields were typically 50−97% before purification. Products from both steps were analyzed via ^{1}H and ^{13}C NMR on a Bruker 200 MHz NMR using deuterated DMSO as the solvent and TMS as the internal reference. The maleamic acids were characterized by a broad peak due to the acid proton near 10−14 ppm, a singlet due to the amide proton near 8−10 ppm, and two doublets due to the ene protons near 6−7 ppm, relative to TMS in the proton spectra. The maleamic acids were also characterized by two peaks near 165 ppm due to the amide and acid carbonyls in the carbon spectra. The maleimides were characterized by the absence of the acid and amide proton peaks, and the single ene proton peak shifted to about 7.6 ppm in the proton spectrum. In the carbon spectrum, the maleimide typically shows a single carbonyl peak near 170 ppm. Peak shifts for each of the N-aromatic maleimides synthesized follow.

N-(2,6-Diisopropylphenyl)maleimide (26DIPPMI): ^{1}H NMR (d_6-DMSP, TMS; δ, ppm) 1.06 doublet, 2.57 multiplet, 7 multiplet, 7.5 multiplet; ^{13}C NMR (d_6-DMSP, TMS; δ, ppm) 23.57 singlet, 28.56 singlet, 123.74 singlet, 126.51 singlet, 129.89 singlet, 134.81 singlet, 147.16 singlet, 170.83 singlet.

N-(2-*tert*-Butylphenyl)maleimide (2tBPMI): ^{1}H NMR (d_6-DMSP, TMS; δ, ppm) 1.22 singlet, 7.1−7.6 multiplet; ^{13}C NMR (d_6-DMSP, TMS; δ, ppm) 31.20 singlet, 127.1 singlet, 128.1 singlet, 129.5 singlet, 131.9 singlet, 135.5 singlet, 149.0 singlet, 171.2 singlet.

N-(2-Phenylphenyl)maleimide (2PPMI): ^{1}H NMR (d_6-DMSP, TMS; δ, ppm) 3.33 doublet, 7.1 multiplet, 7.4 multiplet; ^{13}C NMR (d_6-DMSP, TMS; δ, ppm) 127.6 singlet, 127.7 singlet, 128.4 singlet, 129.0 singlet, 129.6 singlet, 130.0 singlet, 130.4 singlet, 134.8 singlet, 138.3 singlet, 141.0 singlet.

N-(2-Fluorophenyl)maleimide (2FPMI): ^{1}H NMR (d_6-DMSP, TMS; δ, ppm) 7.27 singlet. 7.0−7.6 multiplet; ^{13}C NMR (d_6-DMSP, TMS; δ, ppm) 116.2 singlet, 116.5 singlet, 129.9 singlet, 130.6 singlet, 130.9 singlet, 131.1 singlet, 135.2 singlet, 169.2 singlet.

N-(2-Chlorophenyl)maleimide (2ClPMI): ^{1}H NMR (d_6-DMSP, TMS; δ, ppm) 7.28 singlet, 7.0−7.7 multiplet; ^{13}C NMR (d_6-DMSP, TMS; $\delta\delta$, ppm) 128.2 singlet, 129.2 singlet, 129.9 singlet, 131.0 singlet, 131.5 singlet, 132.2 singlet, 135.0 singlet.

N-(2-Bromophenyl)maleimide (2BrPMI): ^{1}H NMR (d_6-DMSP, TMS; δ, ppm) 7.28 singlet, 7.5 multiplet, 7.8 multiplet; ^{13}C NMR (d_6-DMSP, TMS; δ, ppm) 122.9 singlet, 128.7 singlet, 131.0 singlet, 131.3 singlet, 131.6 singlet, 133.0 singlet, 135.1 singlet.

N-(2-Iodophenyl)maleimide: ^{1}H NMR (d_6-DMSP, TMS; δ, ppm) 7.0−7.3 multiplet, 7.3−7.6 multiplet, 8.0 doublet; ^{13}C NMR (d_6-DMSP, TMS; δ, ppm) 100.4 singlet, 129.3 singlet, 131 singlet, 134.8 singlet, 135.1 singlet, 139.1 singlet, 169.2 singlet.

N-(2-Bromo-3,5-bis(trifluoromethyl)phenyl)maleimide (2Br35CF3PMI): ^{1}H NMR (d_6-DMSP, TMS; δ, ppm) 7.40 singlet, 8.30 singlet, 8.45 singlet; ^{13}C NMR (d_6-DMSP, TMS; δ, ppm) 119.2 singlet, 124.6−126.9 multiplet, 129.3−132.3 multiplet, 135 doublet. (There is possible contamination of NMR sample by residual toluene.)

N-(4-Trifluoromethylphenyl)maleimide (4CF3PMI): ^{1}H NMR (d_6-DMSP, TMS; δ, ppm) 7.25 singlet, 7.62 doublet, 7.88 doublet; ^{13}C NMR (d_6-DMSP, TMS; δ, ppm) 125.9 singlet, 126.9 doublet, 134.9 singlet, 169.5 singlet.

N-(2-Trifluoromethylphenyl)maleimide (2CF3PMI): ^{1}H NMR (d_6-DMSP, TMS; δ, ppm) 7.30 singlet, 7.6−8.0 multiplet; ^{13}C

NMR (d_6-DMSP, TMS; δ, ppm) 127.2 singlet, 130.4 singlet, 132.4 singlet, 133.9 singlet, 135.4 singlet, 169.7 singlet.

N-(2-Trifluoromethylphenyl)citraconimide (2CF3PCI): ^{1}H NMR (d_6-DMSP, TMS; δ, ppm) 2.11 singlet, 6.90 triplet, 7.6−7.3 multiplet; ^{13}C NMR (d_6-DMSP, TMS; δ, ppm) 120.3 singlet, 125.7 singlet, 127.1 singlet, 127.2 singlet, 127.9 singlet, 128.3 singlet, 128.5 singlet, 129.1 singlet, 129.9 singlet, 130.3 singlet, 132.3 singlet, 133.9 singlet, 146.4 singlet, 169.4 singlet, 170.4 singlet.

N-(2-Trifluoromethylphenyl)itaconimide (2CF3PII): ^{1}H NMR (d_6-DMSP, TMS; δ, ppm) 3.76 singlet, 4.0 doublet, 6.2 singlet, 6.7 triplet, 8.0−8.3 multiplet; ^{13}C NMR (d_6-DMSP, TMS; δ, ppm) 34.1 singlet, 120.9 singlet, 127.1 singlet, 127.6 singlet, 130.4 singlet, 131.5 singlet, 134.0 singlet, 168.6 singlet, 173.2 singlet.

2. UV−Vis Absorption Spectroscopy. UV−vis absorption spectra were measured using a Cary 500 Scan UV−vis near-IR spectrophotometer by Varian. Solvents for the UV−vis spectral analyses were primarily Burdick and Jackson brand, except for some cases in which Optima acetonitrile was used. Standard quartz cells were used.

3. Laser Flash Photolysis (LFP) Spectroscopy. LFP was performed using a Continuum Surelite Nd:YAG laser excitation source and a UV−vis absorption/emission monitoring system from Applied Photophysics. Excitation wavelengths of 355 and 266 nm were used with laser energies of approximately 160 and 70 mJ, respectively. Samples were prepared in CH_3CN solution to have an optical density (OD) of 1.0 at the excitation wavelength in 1 cm quartz cells. The UV−vis absorbance at specific wavelengths was measured for each sample before the laser pulse (∼15 ns duration) and as a function of time after the laser pulse. Exponential fits of the resulting absorbance decay curves allowed calculation of the lifetimes of the transient excited-state species. The transient absorbance and lifetimes were measured as a function of monitoring wavelength, allowing reconstitution of the time-resolved UV−vis absorption spectrum of the transient excited-state species. Measurement of the transient lifetime at the transient absorption peak maximum as a function of quencher concentration allows calculation of the Stern−Volmer quenching rate constant (k_q) through

$$\tau_0/\tau = 1 + k_q\tau_o[Q] \qquad (1)$$

where τ_o is the lifetime in the absence of quencher, τ is the lifetime at a given quencher concentration [Q], $k = 1/\tau$ is the rate for transient decay at a given [Q], $k_0 = 1/\tau_0$ is the rate for transient decay in the absence of quencher, and k_q is the rate constant for quenching (L mol^{-1} s^{-1}).

4. Single-Crystal X-ray Diffraction (SCXD). SCXD was performed using a Siemens R3m/V single-crystal X-ray diffractometer, with a Mo Kα X-ray source producing radiation with a wavelength of 7.1073×10^{-11} m. The positions of all non-hydrogen atoms were determined with direct methods (G. Sheldrick, 1993)[12] and refined by full-matrix least-squares (G. Sheldrick, 1997).[13] Hydrogen atom positions were found in difference Fourier maps and placed in calculated positions. The resolution of the determinations in each case was below 0.7 Å, and hydrogen atoms in C−H bonds were resolved, though they are thermal and the distances are affected by the usual distortions associated with the nonspherical character of the hydrogen atom electron density. Complete structural data including cell constants and bond distortions will be published separately.

5. Photo-Differential Scanning Calorimetry (Photo-DSC). Photo-DSC was typically performed on a Perkin-Elmer DSC-7 modified with quartz windows in the sample head cover and a shuttered 450 W medium-pressure mercury lamp. On-sample light intensities were maximal at about 50 mW/cm^2, with lower intensities obtained by using neutral density filters or by increasing the distance between the lamp and DSC head. Specific spectral bands were isolated using band-pass filters, typically 313 and 365 nm. Samples of 2 μL were added to specially crimped aluminum DSC pans, leading to a theoretical sample thickness of about 190 μm, and were purged with nitrogen for 2.5 min prior to and during irradiation. Exotherm peak maxima are proportional to the relative maximum rates of polymerization, and peak integrations are proportional to the monomer conversion. Some exotherm data were acquired using a Mettler-Toledo Star System DSC modified by the addition of a Hammamatsu high-pressure xenon-doped Hg light source and a quartz sample cell cover. The light intensity was set at 50 mW/cm^2 for the experiments with the Mettler system.

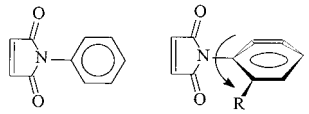

Figure 4. Planar and twisted conformations of ARMIs.

Results and Discussion

Initial examination of N-aromatic maleimides in our laboratories led to the presumption that they were incapable of initiating free radical polymerization. Literature reports[14,15] that the UV−vis absorption spectra and fluorescence emission spectra of N-aromatic naphthalimides closely resembled the absorption and emission spectra of *N*-alkylnaphthalimides upon substitution of a bulky group in the ortho position of the phenyl ring led to the presumption that forcing the maleimide ring to be antiplanar with respect to the phenyl ring (Figure 4) might change the photophysical and photochemical properties of ARMIs such that they would initiate polymerization similarly to N-aliphatic maleimides. To test this hypothesis, photophysical and photochemical studies of a series of ARMIs were performed and the results correlated with relative photoinitiation efficiencies inferred from photo-DSC polymerization exotherms.

1. Single-Crystal X-ray Diffraction. SCXD analysis of single crystals of all of the ARMIs (except for 4CF3PMI, which could not be crystallized to give a single crystal suitable for X-ray analysis) allowed calculation of the torsion angles between the maleimide ring and the phenyl ring in the crystalline state. Torsion angles (τ) and experimental UV−vis absorption spectra for five of these compounds (PMI, 2FPMI, 2ClPMI, 2BrPMI, and 2IPMI) were recently compared[16] to torsion angles and calculated UV absorption spectra based upon energy-minimized conformations from semiempirical AM1 and ab initio SCF, DFT, and MP2 calculations. Conformational energy minima were compared to conformational energies calculated at $\tau = 0°$ and $\tau = 90°$. Good correlation was found between the experimentally observed torsions and UV absorption bands and the calculated minimized torsions and UV absorption bands. Ortho substituents larger than fluorine were found to significantly increase the conformational energy, indicating that the $\tau = 0°$ conformation is not possible without significant molecular distortion. Torsion angle data previously reported for these five ARMIs are included for comparison with the remaining nine ARMI torsion analyses. 2FPMI exhibited a disorder in the position of the fluorine that may occupy either of the equivalent ortho positions in one of the two conformers in the repeating unit cell. This disorder is not uncommon for *o*-fluorophenyl compounds, and the torsion angles for the two major conformers

TABLE 1: Torsion Angles Calculated from SCXD Crystal Structure Determinations

compd	τ (deg)	compd	τ (deg)
Ortho-Substituted ARMIs			
26DIPPMI	84.5	2FPMI	54.1, 66.8
26DIPPMI (benzene solvate)	85.4	2ClPMI	66.1
2tBPMI	88.6	2BrPMI	67.8
2CF3PMI	86.6	2IPMI	83.9
2PPMI	79.6	2Br35CF3PMI	88.9
Unsubstituted and Para-Substituted ARMIs			
PMI	49.5	4CF3PMI	*a*
4OCH3PMI	63.7		
Isomaleimide Derivatives			
2CF3PCI	85.5	2CF3PII	85.5

[a] Suitable single crystals could not be obtained.

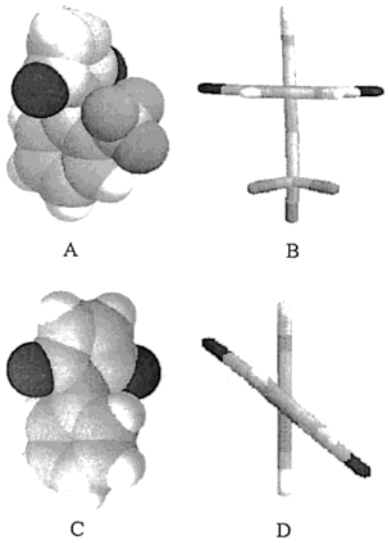

Figure 5. Molecular structure of 2CF3PMI (A, B) and PMI (C, D) as determined by single-crystal X-ray diffraction. (A) and (C) are space-filling models constructed from the atomic coordinates from the crystal structure. (B) and (D) are stick-model projections based upon the crystal structure data looking down the nitrogen−phenyl bond to illustrate the torsion angles.

are given. Torsion angle data for all the structures characterized are given in Table 1 and example structures in Figure 5. Full structural data including cell constants, deformations, and atom coordinates have been submitted separately for publication.

All of the ARMIs examined exhibited a nonzero torsion angle in the crystalline state. In the cases where there is little energetic barrier to molecular planarity, i.e., PMI, 2FPMI, and 4OCH$_3$-PMI, molecular packing energetics may contribute significantly to the final conformation adopted in the crystalline state. Generally, the larger the ortho substituent, the closer the torsion angle approaches $\tau = 90°$, as expected. While the torsion angles in solution may be different from those observed in the crystalline state, there is little doubt that ARMIs with substituents larger than fluorine or chlorine must have $\tau \gg 0°$, i.e., must be "twisted", in gas and solution, as well as in the solid state. As will be discussed, changes in molecular conformations result in partial isolation of chromophores; i.e., the phenyl ring and the imide ring, give rise to changes in the photophysical properties of the molecules such as UV−vis absorption spectra and laser flash photolysis transient absorption spectra, and alter their photoinitiation characteristics.

2. UV−Vis Absorption. The absorption characteristics of N-substituted ARMIs have been reported.[17] To gain additional insight into the nature of ARMI excited states, all of the ARMIs as well as MMI were characterized using UV−vis spectral analysis as a function of solvent polarity. Data for 2IPMI and 2Br35CF3PMI were excluded because overlap of the longest wavelength absorption band (primarily on the imide ring) with the shorter wavelength absorption near 270 nm (primarily localized on the phenyl ring) prevented determination of an accurate peak maximum and extinction coefficient for the longer wavelength band. Peak maxima and molar extinction coefficients at the peak maxima of the lowest observed absorption bands of both planar and twisted ARMIs are given in Table 2 in acetonitrile (CH_3CN), dichloromethane (CH_2Cl_2), and chloroform ($CHCl_3$). We note that 4CF3PMI, for which no SCXD data were obtained, can be classified as planar on the basis of its spectral characteristics. Average molar extinction coefficients as well as average solvent shifts for the two ARMI groups (twisted and planar) are compared in Table 3. Three other planar ARMIs with single substituents (CH_3, CN, and $COOCH_3$) were also evaluated and gave UV spectral results consistent with those reported in Table 2.

TABLE 2: Longest Wavelength UV Absorption Peak Maxima and Molar Extinction Coefficients for MMI and ARMIs as a Function of Solvent Polarity[a]

compd	solvent	peak max (nm)	ϵ at peak max (L mol^{-1} cm^{-1})
MMI	$CHCl_3$	299	826
	CH_2Cl_2	298	821
	CH_3CN	298	732
Twisted ARMIs			
2CF3PMI	$CHCl_3$	286	639
	CH_2Cl_2	286	568
	CH_3CN	287	488
26DIPPMI	$CHCl_3$	293	597
	CH_2Cl_2	293	551
	CH_3CN	293	425
2ClPMI	$CHCl_3$	290	522
	CH_2Cl_2	289	519
	CH_3CN	289	491
2BrPMI	$CHCl_3$	288	582
	CH_2Cl_2	287	538
	CH_3CN	287	484
Planar ARMIs			
PMI	$CHCl_3$	318	429
	CH_2Cl_2	314	479
	CH_3CN	307	458
2FPMI	$CHCl_3$	300	620
	CH_2Cl_2	299	508
	CH_3CN	294	513
4CF3PMI	$CHCl_3$	313	542
	CH_2Cl_2	310	508
	CH_3CN	304	471
4OCH3PMI	$CHCl_3$	340	244
	CH_2Cl_2	331	290
	CH_3CN	315	306

[a] $CHCl_3$, CH_2Cl_2, and CH_3CN have dielectric constants of 4.81, 9.08, and 37.5, respectively.

Matsuo[17] suggested that, as the N-substituent on maleimides is changed from planar phenyl, to alkyl, to hydrogen, the hybridization on the nitrogen nonbonding orbital changes from pure p type to sp^3 type, with a concomitant increase in the overlap of the oxygen lone pair (n) orbital with the nitrogen orbital, resulting in a perturbation of the n $\rightarrow \pi^*$ transition on the carbonyl by an allowed $\pi \rightarrow \pi^*$ transition. Other work on β,γ-unsaturated ketones[18] suggests that overlap between the oxygen orbital on the ketone and the p orbital on the ene can lead to perturbation of the n $\rightarrow \pi^*$ transition by the $\pi \rightarrow \pi^*$ transition on the ene, resulting in an increase in the oscillator strength of the transition, and an intensification of the absorption band. Matsuo suggests that, in the case of ARMIs, there may

TABLE 3: Comparison of the Spectral Features of the Longest Wavelength UV Absorption Bands of Planar and Twisted ARMIs with an *N*-Alkylmalimide (MMI)

compd	av ϵ at peak max (L mol^{-1} cm^{-1})	ϵ at peak max (min, max) (L mol^{-1} cm^{-1})	av Δ peak max ($CHCl_3 \rightarrow CH_3CN$) (nm)	Δ peak max (min, max) (nm)
MMI	793	732, 826	−1	
twisted ARMIs	545	425, 639	−1.1	0, 2
2FPMI	547	508, 620	−6	
planar ARMIs	440	244, 542	−13	9, 25

be analogous overlap of the carbonyl n orbital with the highest occupied π orbital on the phenyl ring when the phenyl ring is nearly planar with respect to the imide ring. He further observed that there is an additional band around 260 nm for ARMIs originating on the phenyl ring.[17] These bands were also observed in spectra measured in this study. Observation of the shift of these bands with increasing solvent polarity shows very small changes. These data along with the rather large molar extinction coefficient ($\sim 10^3$) confirm assignment of the band as a $\pi \rightarrow \pi^*$ transition from the phenyl ring, as predicted in the calculations presented previously.[16]

In the present investigation, UV−vis absorption spectra indicate that the average molar extinction coefficients at the peak maxima of the transition between 275 and 320 nm increase in the order planar phenyl < twisted phenyl < alkylmaleimide (Table 3). The twisted N-aromatic maleimides have an average molar extinction coefficient of the longest wavelength absorption band approximately 24% larger than those of the planar analogues. A reasonable comparison can be made between 2CF3PMI and 4CF3PMI, whose inductive electron-withdrawing effects on the ring should be similar. The molar extinction coefficients are 639 L mol^{-1} cm^{-1} at 285.5 nm and 542 L mol^{-1} cm^{-1} at 312.5 nm for 2CF3PMI and 4CF3PMI, respectively. Both the increase in molar extinction coefficient and the shift to higher energy transition ($\Delta E_{\pi\rightarrow\pi^*} > \Delta E_{n\rightarrow\pi^*}$, in general) agree with the postulate that the transition increases in $\pi \rightarrow \pi^*$ character when the phenyl ring and imide ring are nearly antiplanar. For the compounds evaluated in this investigation, the magnitudes of the extinction coefficients range from a minimum of about 244 L mol^{-1} cm^{-1} for 4OCH3PMI (a planar ARMI with an electron donor group in the para position) to 826 L mol^{-1} cm^{-1} for MMI. These values are not large enough to suggest a pure $\pi \rightarrow \pi^*$ transition, which should have a molar extinction coefficient minimally between 10^3 and 10^4 L mol^{-1} cm^{-1}. They are larger than typical n $\rightarrow \pi^*$ molar extinction coefficients, however, which are typically less than 200 L mol^{-1} cm^{-1}.[19] Our results agree with those of Matsuo,[17] suggesting that the absorption band with peak maxima near 290 nm is principally an n $\rightarrow \pi^*$ transition, increasingly perturbed by an allowed $\pi \rightarrow \pi^*$ transition as the N-substituent is changed from planar phenyl, to twisted phenyl, to alkyl.

UV−vis absorption spectra, obtained for the ARMIs used in this investigation in chloroform ($CHCl_3$), dichloromethane (CH_2Cl_2), and acetonitrile (CH_3CN), with dielectric constants of 4.81, 9.08, and 37.5, respectively, for MMI, 26DIPPMI, and PMI, are given in Figures 6−8, respectively. On the basis of the spectral shift data for all of the ARMIs evaluated, the compounds may be segregated again into two main groups. The first group includes MMI and all the twisted ortho-substituted ARMIs, with the exception of 2FPMI. The compounds in this group show only negligible shifts (see Figures 6 and 7 for examples) upon changing from $CHCl_3$ to CH_3CN. These results are consistent with those reported by Matsuo, who observed a negligible 2−3 nm shift for *N*-ethylmaleimide and *N*-cyclohexylmaleimide when changing from *n*-hexane (dielectric constant 1.89) to CH_3CN (dielectric constant 37.5).[17] The second

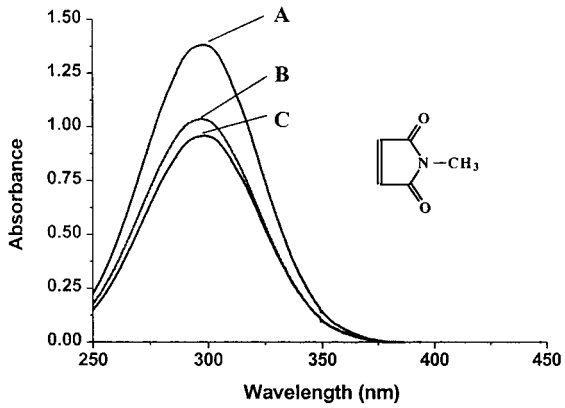

Figure 6. UV−vis absorption spectra of MMI in (A) CH_2Cl_2, (B) CH_3CN, and (C) $CHCl_3$, with concentrations of 1.68×10^{-3}, 1.42×10^{-3}, and 1.16×10^{-3} M, respectively.

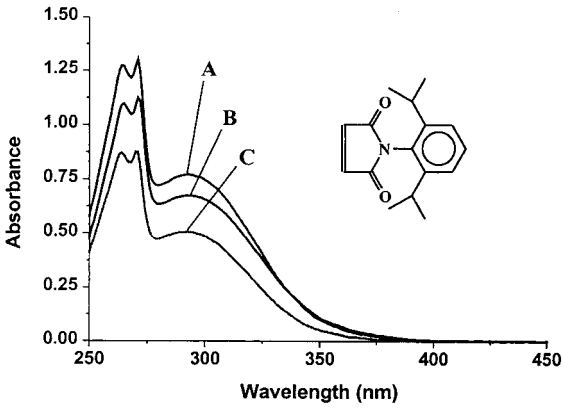

Figure 7. UV−vis absorption spectra of 26DIPPMI in (A) CH_2Cl_2, (B) $CHCl_3$, and (C) CH_3CN, with concentrations of 1.40×10^{-3}, 1.13×10^{-3}, and 1.19×10^{-3} M, respectively.

group, planar ARMIs including PMI and para-substituted ARMIs, on the other hand, exhibit large shifts to shorter wavelengths, ranging in magnitude from 9 to 25 nm. In general, the substituents seemed to affect the magnitude of the shift to shorter wavelength in the order electron-withdrawing < unsubstituted < electron-donating. The largest shift of 25 nm observed for 4OCH3PMI is comparable to the shift of 31 nm obtained by Matsuo[17] for 4OCH3PMI upon changing from hexane to CH_3CN. Shifts of this magnitude are larger than expected simply on the basis of n $\rightarrow \pi^*$ character in the transition, suggesting significant charge-transfer (CT) character in the ground state of planar ARMIs. 2FPMI seems to fall between the two groups, exhibiting extinction coefficients in the same range as the other ortho-substituted ARMIs while giving an intermediate shift magnitude of 6 nm upon changing from $CHCl_3$ to CH_3CN. The fluoro group is small, and the resulting torsion angle in 2FPMI is therefore little different from that of PMI, though the population average conformation of neither compound is likely to be completely planar in the gas or solution phase. Indeed, torsion angle data and semiempirical calculations for conformation energetics and UV−vis absorption bands of compounds in

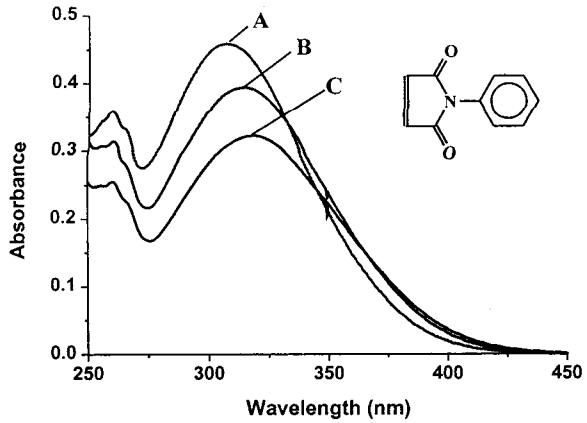

Figure 8. UV−vis absorption spectra of PMI in (A) CH_3CN, (B) CH_2Cl_2, and (C) $CHCl_3$, with concentrations of 9.99×10^{-4}, 8.20×10^{-4}, and 7.51×10^{-4}, respectively.

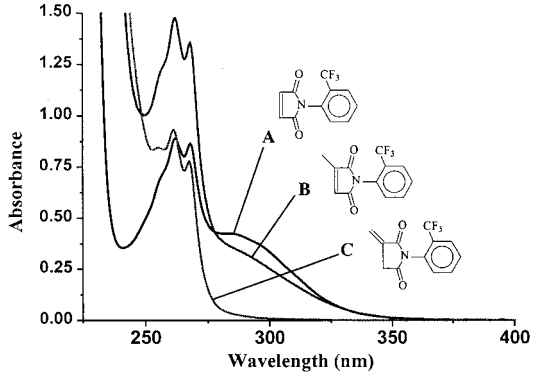

Figure 9. UV−vis absorption spectra of (A) 8.62×10^{-4} M 2CF3PMI, (B) 1.36×10^{-4} M 2CF3PCI, and (C) 8.03×10^{-4} M 2CF3PII in CH3CN.

the series PMI, 2FPMI, 2ClPMI, 2BrPMI, and 2IPMI reported previously[16] confirm this assertion. Matsuo's postulate of a mixed transition, with the n → π^* transition increasingly perturbed by a $\pi \rightarrow \pi^*$ transition in the series planar aromatic < twisted aromatic < alkyl < unsubstituted maleimide,[17] explains our observations.

UV−vis absorption spectra were also measured for two maleimide analogues, 2CF3PCI and 2CF3PII. Comparison of the absorption spectra of these compounds with that of 2CF3PMI in Figure 9 shows that substitution of the methyl group on the double bond (citraconimide) shifts the 280 nm band to shorter wavelength with respect to that of the analogous maleimide. The itaconimide is essentially a substituted acrylamide, and exhibits a longest wavelength peak that is shifted even further toward the 260 nm band.

3. Laser Flash Photolysis. It has been previously reported[1,20] that the transient UV−vis absorption spectra of *N*-alkylmaleimides show a single absorption band with peak maxima near 340 nm that is quenched by oxygen, 1,3-cyclohexadiene, and β-carotene, the latter producing the distinctive triplet absorption spectrum of β-carotene, thus providing conclusive evidence for the triplet state. The transient optical densities, peak maxima, and measured triplet lifetimes for 2CF3PMI, 4CF3PMI, MMI, and eight other ARMIs are given in Table 4. The data are listed in order of decreasing relative transient yield, taken to be the relative optical densities at the transient peak maxima. Representative transient absorption spectra for 2CF3PMI and 4CF3PMI are given in Figures 10 and 11, respectively.

3.1. Transient Spectral Features. The order of the relative yield (relative absorbance of the transients obtained under identical conditions) of transient divides the ARMIs into the same two groups as before, with the exception of 26DIPPMI. The twisted ARMIs generally exhibit a higher relative triplet yield than the planar compounds. The optical densities of the transients with peak maxima at ~340 nm are all significantly lower than that of MMI, suggesting that the relative quantum yields of excited-state triplet upon direct excitation of the ARMIs are significantly smaller than that of MMI, which is in turn significantly smaller than that of benzophenone (BP). The low yield of the transient (excited-state triplet, as will be shown later) of 26DIPPMI may be due to enhanced internal conversion from the excited-state singlet to the ground state, thereby decreasing the excited-state singlet lifetime and resulting in a decreased yield of excited-state triplet. Alternatively, the transient yield may be low due to intramolecular hydrogen abstraction of a tertiary benzylic hydrogen on the isopropyl groups by the carbonyl in the excited-state singlet, thereby reducing the effective triplet yield. The same reaction may also occur in the triplet, though the relatively long lifetime of 833 ns measured for the 26DIPPMI transient may suggest that intramolecular hydrogen abstraction is not a significant deactivation pathway in the triplet state. In any case, the relative triplet yields of the

TABLE 4: Laser Flash Photolysis Transient Absorption Data for MMI and Selected ARMIs

compd	λ_{max} (nm)	OD at λ_{max}	lifetime at λ_{max} (ns)
MMI	340	0.11	159
	Twisted ARMIs (Group 1)		
2IPMI	320, 560	0.037, 0.017	76.9, 118
2Br35CF3PMI	330	0.026	775
2CF3PMI	330	0.017	990
2BrPMI	320	0.012	412
2tBPMI	330	0.010	358
2ClPMI	330	0.0087	323
26DIPPMI	340	0.0047	833
	Planar ARMIs (Group 2)		
4CF3PMI	360, 480	0.0084, 0.0067	388, 346
2FPMI	320, 520	0.008, 0.0063	1070, 862
PMI	340, 480	0.0072, 0.0067	417, 400
4OCH3PMI	320, 520	0.0027, 0.002	a
	Solvent		
CH_3CN Solvent		0.0018	

[a] The transient was too weak to measure an accurate lifetime.

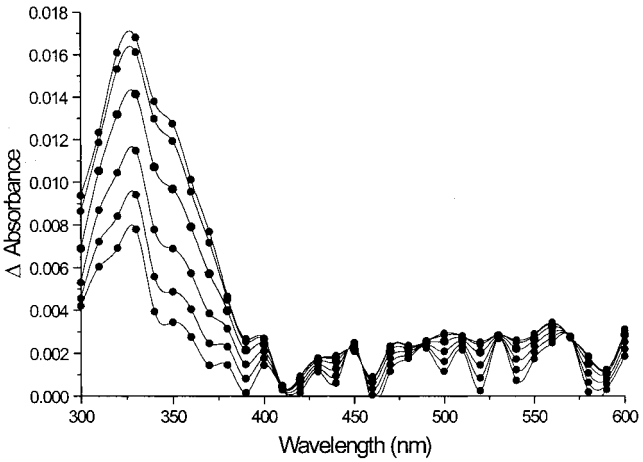

Figure 10. Transient UV−vis absorption spectra for 2CF3PMI in N_2-bubbled CH_3CN with OD = 1 at the excitation wavelength (266 nm). Spectra are given at 50 ns, 100 ns, 250 ns, 500 ns, 750 ns, and 1 μs after the laser pulse. The lifetime at 330 nm was calculated to be 990 ns.

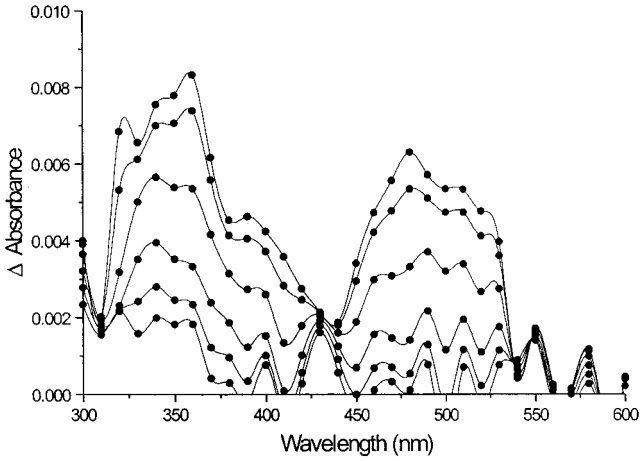

Figure 11. Transient UV−vis absorption spectra for 4CF3PMI in N_2-bubbled CH3CN with OD = 1 at the excitation wavelength (266 nm). Spectra are given at 50 ns, 100 ns, 250 ns, 500 ns, 750 ns, and 1 μs after the laser pulse. The lifetime at 360 nm was calculated to be 388 ns, and the lifetime at 480 nm was calculated to be 346 ns.

ARMIs are all low upon direct excitation, with the planar ARMIs having extremely low yields.

The relative transient yield for 2IPMI (0.037) was more than double that of 2CF3PMI (0.017), and the 2IPMI transient had a significantly shorter triplet lifetime than 2CF3PMI, 77 ns versus 990 ns, respectively. These two observations suggest that triplet-state formation and decay may be influenced by an internal heavy atom effect which increases the rates of intersystem crossing. The effect is generally only significant in $\pi \rightarrow \pi^*$ states, as the spin−orbit coupling effect operative in n $\rightarrow \pi^*$ states is of a much higher magnitude.[19] Heavy atom effects not only increase the triplet yields from excited singlets, but also decrease the triplet-state lifetime by increasing intersystem crossing rates to the ground-state singlet.[19] The lifetime of the 2IPMI triplet may also be decreased due to a possible photocleavage reaction. This is certainly consistent with our observation of a 560 nm peak in the spectrum of 2IPMI attributed to the formation of a transient photoproduct, likely from photocleavage of the phenyl−halogen bond, which is well-known in the literature.[21−23] (Interestingly, the 2IPMI solution was in fact visibly yellow after a time of continuous pulsing, suggesting the possible formation of molecular iodine).

A correlation between the ARMI structure and the shapes of the transient absorption spectra was also observed. The twisted ARMIs all exhibited a single transient peak (Figure 10) similar to that observed in MMI, with the exception of 2IPMI, which showed an additional peak at 560 nm as discussed previously. The planar ARMIs all exhibited a bimodal transient absorption spectrum (Figure 11), generally with peak maxima between 320 and 360 nm and between 480 and 520 nm. The origin of the second transient absorption band has not been determined. Possible explanations include the following: (a) The two bands might be due to a single species. Similarity of the lifetimes at the two peak maxima in the transient spectrum of PMI and 4CF3PMI suggests the possibility of a single excited-state species in each ease. In the case of 2FPMI, the two bands differ in calculated lifetime by about 20% (1070 ns versus 862 ns), which may be within experimental error given the low intensity of the absorption. However, the similarity in lifetimes may simply connote two species with similar or coupled molecular structure. (b) Two distinct populated excited triplet states may exist for planar ARMIs, as in the case of 2-phenylbenzophenone (2PBP) described by Scaiano, where he claimed that two energetically close ($\Delta \approx 4$ kcal/mol) excited triplets states exist for 2PBP, which may interconvert by rotation of one of the phenyl rings.[24] In the case of planar ARMIs, there is little barrier to planarity or perpendicularity of the two rings, vide supra from the AM1 rotational conformer calculations previously reported.[16] Extension of these trends to the planar ARMIs might suggest the existence of two excited-state triplets, i.e., one planar and one perpendicular, which if close enough in energy (~2 kcal/mol in the ground state from AM1) might be equally populated, giving rise to two triplet−triplet absorption bands in the excited state. If the interconversion between the two triplet states is hindered such that the bond rotation does not occur within the lifetimes of the two states, then the two states may be distinct. Further support of the dual excited-state hypothesis comes from reports by Valat et al.,[14,15] who reported that *N*-phenylnaphthalimides with bulky ortho substituents have UV−vis absorption (and fluorescence) very similar to that of *N*-alkylnaphthalimides, while unsubstituted and non-ortho-substituted *N*-phenylnaphthalimides showed red-shifted, with respect to the *N*-alkylnaphthalimides, longest wavelength UV−vis absorption peaks (as well as dual-band fluorescence). After characterizing a host of *N*-alkyl- and substituted *N*-phenylnaphthalimides by UV−vis absorption and fluorescence emission spectroscopies, Valat postulated that two related, yet distinct excited-state singlets are responsible for the two fluorescence emission bands in the non-ortho-substituted *N*-phenylnaphthalimides. Extension of this postulate to the case of ARMIs would suggest that two energetically and conformationally distinct excited singlet states might upon intersystem crossing lead to two distinct excited triplet states. Unfortunately, while fluorescence emission spectra confirmed Valat's postulate in the case of *N*-phenylnaphthalimides, no emission was observed in this investigation of ARMIs. (c) A twisted intramolecular charge-transfer state (TICT) as reported previously for N-aromatic phthalimides[25,26] may be operative for planar N-aromatic maleimides. The lowest possible transition calculated in the AM1 analyses[16] of the *o*-halo-substituted ARMIs was a HOMO to LUMO transition, which was not spatially allowed. The HOMO had π character on the phenyl ring, while the LUMO had π^* character on the maleimide ring double bond and the carbonyls. If such a transition did occur, even with a very low oscillator strength, there would be charge separation because the transition would essentially involve transfer of an electron from an orbital on the phenyl ring to an orbital on the maleimide ring. The excited singlet TICT state might be stabilized through intersystem crossing to an excited TICT triplet state.

Either of the latter two possible explanations for the origin of the second transient absorption band provides for the formation of two distinct excited-state triplet species for planar ARMIs. Further elucidation of these hypotheses for ARMIs is exceedingly difficult in the absence of fluorescence and phosphorescence emission spectra. High-level excited-state triplet to upper excited-state triplet calculations are in progress to attempt to reproduce the UV−vis absorption spectra of the ARMI triplet transients, and will be reported in a future publication.

3.2. Quenching of ARMI Transients. To prove whether the transient species formed upon photolysis of ARMIs were excited-state triplets, quenching studies were performed. Cyclohexadiene (CHD), which has a low-lying triplet state and therefore selectively quenches excited-state triplets, was chosen to quench the *N*-phenylmaleimide transients. Solutions were prepared for PMI and 2CF3PMI, representing planar and twisted ARMIs, respectively, containing various concentrations of CHD.

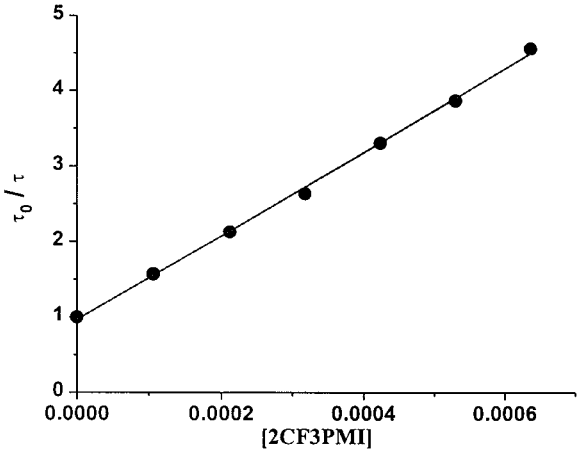

Figure 12. Stern−Volmer analysis of data from quenching BP with 2CF3PMI in CH_3CN solution excited at 355 nm and analyzed at 520 nm following nitrogen purge. The average k_q was determined to be 4.04×10^9 L mol^{-1} s^{-1} on the basis of four replicate data sets with a standard deviation of 9.8×10^7 L mol^{-1} s^{-1}. The average R^2 for the four least-squares fits is 0.999.

TABLE 5: Rate Constants for Quenching of Benzophenone by MMI and Selected ARMIs

quencher	k_q (L mol^{-1} s^{-1})	quencher	k_q (L mol^{-1} s^{-1})
MMI	7.8×10^9	4CF3PMI	2.9×10^9
PMI	3.0×10^9	26DIPPMI	2.2×10^9
2CF3PMI	4.0×10^9		

LFP measurements were performed under conditions similar to those described above. Since the ARMIs had inherently low transient yields, quantitative quenching to obtain quenching rate constants was impossible. Qualitatively, low concentrations of CHD were found to completely quench the transient species observed in 2CF3PMI and PMI (both peaks), strongly suggesting that the transient is the excited-state triplet, as in the case of MMI. In the case of PMI, quenching of both bands suggests that (a) the bands are due to a single triplet species which is quenched, (b) there are two separate excited-state triplets which are both quenched, or (c) that the higher energy band is a triplet which produces the lower energy band species and that quenching of the former prevents formation of the latter. A reduction in the lifetime and intensity of the transient absorption bands for both PMI and 2CF3PMI in air-saturated solutions suggests oxygen quenching of excited-state triplets. These observations, along with inferences from MMI experiments,[2] provide strong evidence for the characterization of the transient absorption species of ARMIs as excited-state triplets.

3.3. Quenching of Benzophenone by Triplet ARMIs. A targeted application of the research on ARMIs in this investigation is the photoinitiation of radical polymerization in the presence of absorbing compounds which may act, in part, as sensitizers for triplet formation of ARMIs. Elucidation of the relative efficiencies of triplet sensitization of maleimide triplets by benzophenone is therefore of great interest. To this end, solutions were prepared containing BP with increasing concentration of various maleimides to determine the rate constants for quenching (k_q) of the excited-state BP triplet by the maleimides. The lifetime of the BP triplet was measured as a function of the concentration of the quencher, and the data were plotted using the Stern−Volmer relation[19] (as in Figure 12 for CF3PMI). Quenching constants (k_q) determined from such Stern−Volmer plots are given in Table 5. The rate constants for quenching of BP excited-state triplet by ARMIs range from 2.2×10^9 to 4.0×10^9 L mol^{-1} s^{-1} compared to 7.8×10^9 L mol^{-1} s^{-1} for MMI. The quenching constants in Table 5 are all quite large and approach the diffusion-controlled rate of $\sim 10^{10}$ L mol^{-1} s^{-1}. Sensitization of the maleimide triplets by BP could not be confirmed by laser flash transient absorption spectra due to overlap of the BP 310 nm band with the maleimide bands, as well as competitive absorption by the maleimides, resulting in production of the maleimide transient by direct excitation. Quenching of the 2CF3PMI transient (formed upon direct excitation in the absence of BP) by *N*-methyl-*N*,*N*-diethanolamine (MDEA) showed that the maleimide triplet was quenched by the amine, though calculation of a k_q for the reaction was problematic due to the inherently low transient absorbance of 2CF3PMI.

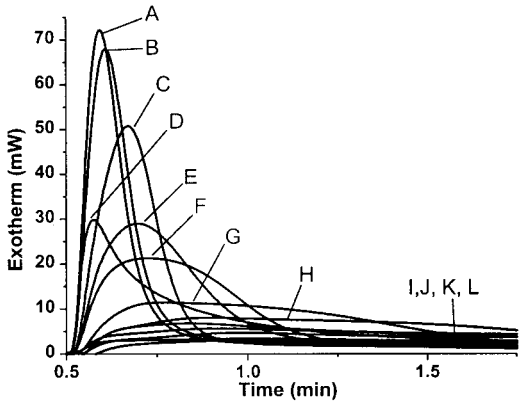

Figure 13. Photo-DSC exotherms from the photopolymerization of PEG400DA initiated by approximately 5 mol % N-substituted maleimides, based upon the mole percent of the compound: (A) 4.97% 2Br35CF3PMI, (B) 5.01% 2IPMI, (C) 5.01% MMI, (D) 4.96% BP, (E) 4.99% 2CF3PMI, (F) 4.99% 2BrPMI, (G) 5.01% 2ClPMI, (H) 5.00% 26DIPPMI, (I) 5.02% 2tBPMI, (J) 4.99% 2FPMI, (K) 4.97% 4CF3PMI, (L) 4.97% PMI. Samples of 2 μL were polymerized under nitrogen at 25 °C using the full arc of the medium-pressure mercury lamp with an on-sample light intensity of 32.2 mW/cm^2. Samples were not normalized for initiator absorbance.

4. Photopolymerization. *4.1. Direct Exposure of N-Alkylmaleimides and N-Aromatic Maleimides*. As discussed in the Introduction, *N*-alkylmaleimides have been shown to initiate free radical polymerization by a hydrogen abstraction process in the presence of a hydrogen atom donor synergist.[1,2] The hydrogen atom donor may be added directly to the formulation as a synergist, or incorporated into the monomers. In the case of PEG400DA, which is a diacrylate with an average of 10 ethylene oxide units in the spacer group, the hydrogen atoms on the carbons α to the ether oxygens are labile, and readily abstracted by hydrogen-abstraction-type photoinitiators. Accordingly, PEG400DA was found to photopolymerize readily in the presence of *N*-alkylmaleimides and certain N-aromatic maleimides, with the efficiency of the initiation depending upon the maleimide structure. As shown by the photo-DSC exotherms in Figure 13 for 10 ARMIs, selected from those depicted in Figure 2 as well as for MMI and BP, the highest relative polymerization efficiencies, i.e., exotherm peak maxima, were obtained for samples with 2Br35CF3PMI and 2IPMI followed by the sample with MMI. The exotherms for the six maleimides of lowest reactivity are either less than or not significantly higher than the exotherm measured for neat PEG400DA, which self-initiates perhaps by excitation of peroxide impurities or acrylate groups directly. Interestingly, 2IPMI and 2Br35CF3PMI exhibited the highest triplet yield of the ARMIs, though significantly less than that of MMI (Table 4). The polymerization rates obtained for 2CF3PMI- and BP-initiated samples were significantly lower than those for MMI, 2IPMI, or 2Br35CF3PMI. It

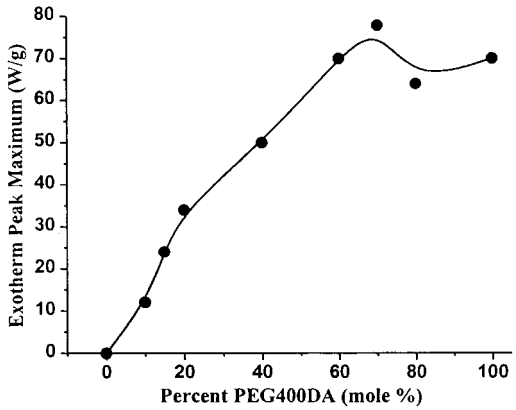

Figure 14. Photo-DSC exotherm peak maxima for the polymerization of HDDA/PEG400DA formulations initiated by 5 mol % 2CF3PMI, based upon the moles of the functional groups, as a function of PEG400DA content. Samples of 2 μL were irradiated at 25 °C under nitrogen atmosphere by the full arc output of a xenon-doped high-pressure mercury lamp with an on-sample light intensity of 50 mW/cm^2.

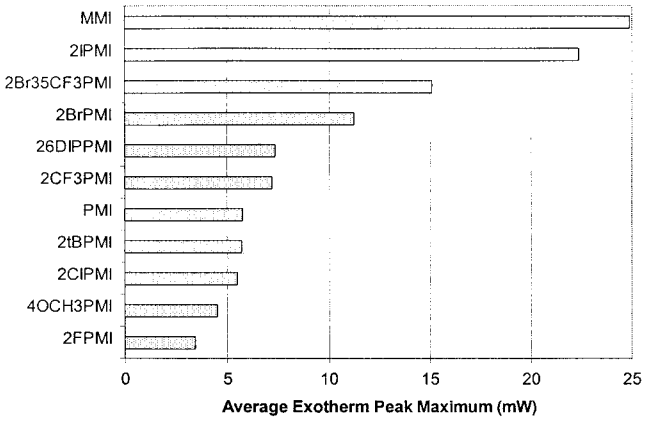

Figure 15. Photo-DSC exotherm peak maxima for HDDA initiated by 5 mol % MMI and various ARMIs in the presence of 1 mol % MDEA. Polymerizations were performed using 2 μL samples at 25 °C under nitrogen atmosphere with the full arc of a medium-pressure mercury lamp giving on-sample light intensity of 29.5 mW/cm^2. 4OCH3PMI did not completely dissolve at the concentration and temperature used.

should be noted that the absorbances of initiator in this series were not identical; thus, the initiation efficiencies cannot strictly be compared quantitatively. Ignoring BP, the ranking of polymerization efficiency does however appear to generally follow the order of relative triplet yield with one noted exception, MMI. The molar extinction coefficient of MMI at 266 nm, a principal band in the medium-pressure mercury spectrum, is approximately a factor of 3 smaller than those observed for 2IPMI and 2Br35CF3PMI. However, counterbalancing this effect is the fact that MMI has a significantly higher, by a factor of 3, relative yield of triplet compared to the highest ARMIs, 2IPMI and 2Br35CF3PMI, with relative triplet yields of 0.11 versus 0.037 and 0.026, respectively. Finally, the increased apparent initiation efficiencies, ~40% higher than MMI, of 2IPMI and 2Br35CF3PMI may also be partially due to photocleavage reactions, inferred in the case of 2IPMI from the LFP experiments, generating highly reactive phenyl radicals.

The polymerization efficiency of binary mixtures of HDDA and PEG400DA were found to increase when photoinitiated with 5 mol % 2CF3PMI (Figure 14). The maximum polymerization rate was found to occur for a system with about 70% PEG400DA. The mixtures with higher concentrations of PEG400DA polymerize slower, presumably as a result of the slower inherent polymerization rate of PEG400DA compared to HDDA. HDDA, which has no readily abstractable hydrogens, would not be expected to polymerize efficiently in the presence of N-substituted maleimides without the presence of a source of labile hydrogens. The efficiency of initiation of HDDA, which as noted above has no readily abstractable hydrogens, by *N*-alkylmaleimides has been shown[2] to be enhanced significantly by the addition of an amine due to a highly efficient electron/proton-transfer process. To compare results for the ARMIs with those of *N*-alkylmaleimides, photo-DSC exotherms of samples containing 5 mol % of a series of ARMIs in HDDA with 1 mol % MDEA were measured (Figure 15). The relative ranking of the exotherm peak maxima roughly follows the relative yield of triplet transient measured in the laser flash photolysis experiments (Table 4), with the exceptions of 2CF3PMI and 26DIPPMI. Interestingly, only MMI, 2IPMI, and 2Br35CF3PMI initiators gave polymerization exotherms larger than that of HDDA with amine only (the species responsible for the inherent initiation in the HDDA is probably reduced by competitive absorption of the maleimides). The reason for the low efficiency of twisted ARMIs (with the exception of 2IPMI and 2Br35CF3-PMI) in the presence of MDEA is unknown, although a contributing factor may be a ground-state charge-transfer complex formed between MDEA and the N-aromatic maleimides.

4.2. Exposure of N-Alkylmaleimides and N-Aromatic Maleimides in the Presence of Benzophenone. The quantum yields of excited-state triplet formation of *N*-alkylmaleimides upon direct excitation have been reported by De Schryver and Put[6] to be about 0.23−0.24. A recent publication suggests these values to be even lower.[27] As determined by LFP described in this paper, triplet yields for ARMIs are significantly lower that those for *N*-alkylmaleimides. Photolysis of maleimides in the presence of BP or isopropylthioxanthone (ITX) has been reported to enhance [2+2] cycloaddition[5−11] and free radical initiation of acrylic systems with *N*-alkylmaleimide/amine combinations present.[1,2] Representative photo-DSC exotherms in Figure 16 for several ARMI systems illustrate that both planar and twisted ARMIs exhibit enhanced radical polymerization rates of HDDA in the presence of MDEA when BP is added. All of the maleimides, including *N*-alkylmaleimides as well as twisted and planar ARMIs, exhibited polymerization efficiencies significantly larger than that for the BP/MDEA combination alone in HDDA. Two possibilities for enhanced rates exist. First, as suggested by the laser flash photolysis results in section 3.3, BP may sensitize formation of the maleimide triplet state. Second, recent results from our lab indicate that semipinacol radicals formed from the electron/proton-transfer reduction process involving the BP triplet state and MDEA readily react with (more exactly, are quenched by) N-aromatic maleimides, presumably by an electron/proton-transfer process, to generate BP and the succinimidyl radical. We suppose that both processes for generation of two initiating radicals (both processes produce the same radicals) may take place depending upon the concentration of individual components (maleimide, amine). Elucidation of the mechanistic details is in progress and will be reported in a subsequent publication.

Finally, polymerization of HDDA in the presence of BP (3 wt %), MDEA (1 wt %), and isomaleimides, 2CF3PCI and 2CF3PII (0.1 wt %), indicate that 2CF3PCI/MDEA/BP and 2CF3PII/MDEA/BP systems also operate as efficient free radical initiators. Qualitatively, 2CF3PII does not yield rates of initiation

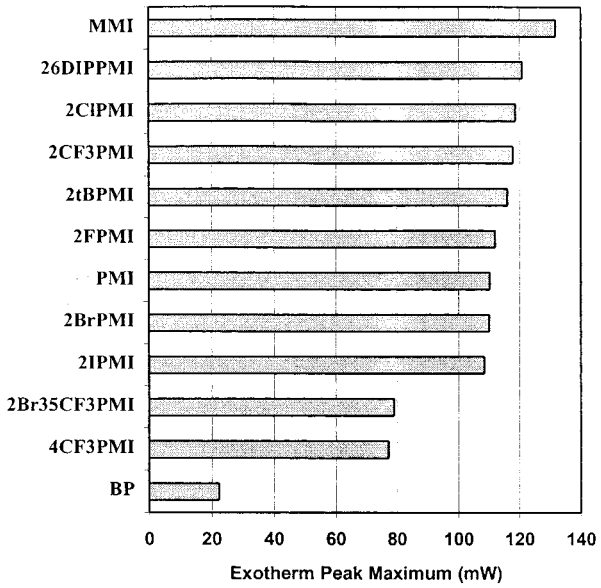

Figure 16. Photo-DSC exotherm peak maxima for HDDA formulations initiated by ARMIs in the presence of an amine and BP. Samples contain 3 mol % BP, based on the moles of the compound, 1% MDEA and 0.10% maleimide, except for the BP sample, which has no maleimide. Samples of 2 μL were polymerized at 25 °C under nitrogen atmosphere, with an on-sample light intensity of 1.86 mW/cm^2 at 365 nm, from the full arc spectrum of a medium-pressure mercury light source.

as high as those found for 2CF3PCI and the other ARMIs. This is not unexpected, however, since the itaconimide resembles a substituted acrylamide much more than a maleimide, and may yield radicals that have different reactivity toward initiation of acrylate polymerization than the maleimide radicals and/or are formed with different efficiencies in the presence of amines or sources of abstractable hydrogens.

Conclusions

N-aromatic maleimide derivatives were evaluated as free radical photoinitiators for acrylate polymerization. The ARMI compounds investigated in this study may be segregated into two groups on the basis of molecular conformation (torsion angle between phenyl and imide rings), UV−vis absorption spectral features, transient UV−vis absorption spectral features observed by laser flash photolysis, and relative photoinitiation efficiency. The first group is composed of ARMIs that are substituted in the ortho position of the phenyl ring by a group sufficiently large (larger than fluorine) to force the average molecular conformation to exist with the imide ring antiplanar with respect to the phenyl ring. These twisted ARMIs exhibited UV−vis absorption spectra similar to that of *N*-alkylmaleimides, with spectral shifts as a function of solvent polarity indicative of a primarily $\pi \rightarrow \pi^*$ longest wavelength absorption band. Transient UV−vis absorption spectra of the excited-state triplet species of the twisted ARMIs very closely resemble the transient spectra observed for *N*-alkylmaleimides. The second group of ARMIs do not have substituents in the ortho position on the phenyl ring, such that there is little conformational energy barrier to forming a planar molecular conformation. These planar ARMIs exhibit longest wavelength UV−vis absorption bands that occur at lower energies than the corresponding bands in the twisted ARMIs and *N*-alkylmaleimides as well as large spectral shifts upon changes in solvent polarity, indicative of a primarily n $\rightarrow \pi^*$ transition or possibly an intramolecular charge-transfer process in certain para-substituted ARMIs. Transient UV−vis absorption spectra for the excited-state triplets of the planar ARMIs show much lower relative triplet-state quantum yields and exhibit a dual-band absorption, in contrast to twisted ARMIs and *N*-alkylmaleimides. The origin of the second transient absorption band is unknown, though arguments were presented suggesting the existence of two distinct excited-state triplet species for planar ARMIs.

Photopolymerization studies indicated that twisted ARMIs efficiently initiate free radical acrylate polymerization in the presence of a hydrogen atom donor synergist upon direct excitation, while planar ARMIs do not. Relative initiation efficiencies generally correlate with the relative yields of excited-state triplet. Addition of benzophenone was found to dramatically increase the initiation efficiencies of both planar and twisted ARMIs. The increase in rate with addition of benzophenone was found to be independent of the maleimide structure (planar ARMI, twisted ARMI, or *N*-alkylmaleimide). This is particularly interesting since *N*-alkylmaleimide/amine/benzophenone systems were previously shown to exhibit initiation efficiencies approaching those of conventional cleavage photoinitiators.[1] Hence, with noted exception, any N-substituted maleimide can be used along with benzophenone or closely related diaryl ketones to initiate acrylate polymerization with efficiencies comparable to those exhibited by cleavage photoinitiators.

Acknowledgment. We gratefully acknowledge the financial support of Fusion UV-Curing Systems and ChemFirst Fine Chemicals. We thank Jeffrey Zubkowski, Department of Chemistry, Jackson State University, for access to the diffraction facility, and the Office of Naval Research (E.J.V.).

References and Notes

(1) Hoyle, C. E.; Viswanathan, K.; Clark, S. C.; Miller, C. W.; Nguyen, C.; Jönsson, S.; Shao, L. *Macromolecules* **1999**, *32*, 2793.

(2) Clark, S. C. Ph.D. Dissertation, Department of Polymer Science, The University of Southern Mississippi, Hattiesburg, MS, 1999.

(3) Sonntag, J. V. Ph.D. Dissertation, Faculty of Chemistry and Mineralogy, The University of Leipzig, Germany, 1999.

(4) Morel, F.; Decker, C.; Jönsson, S.; Clark, S. C.; Hoyle, C. E. *Polymer* **1999**, *40*, 2447.

(5) White, J. E.; Dehnke, M. K.; Tang, L. H. U.S. Patent 4,851,454, 1989.

(6) Put, J.; DeSchryver, F. C. *J. Am. Chem. Soc.* **1973**, *95*, 137.

(7) Meir, K.; Zweifel, J. *J. Photochem.* **1986**, *35*, 353.

(8) DeSchryver, F. C.; Feast, W. J.; Smets, G. *J. Polym. Sci., Part A-1* **1970**, *8*, 1939.

(9) Boens, N.; DeSchryver, F. C.; Smets, G. *J. Polym. Sci., Polym. Chem. Ed.* **1975**, *13*, 201.

(10) Zweifel, H. *Photogr. Sci. Eng.* **1983**, *27*, 114.

(11) Timpe, H.-J. *Proceedings of the Academic Day, Radtech Europe '97*; 1997; p 127.

(12) Sheldrick, G. SHELXS-93, A program for the solution of crystal structures from diffraction data, University of Göttingen, Göttingen, Germany.

(13) Sheldrick, G. SHELXL-97, A program for the refinement of crystal structures from diffraction data, University of Göttingen, Göttingen, Germany.

(14) Valat, P.; Wintgens, V.; Kossanyi, J.; Biczok, L.; Demeter, A.; Berces, T. *J. Am. Chem. Soc.* **1992**, *114*, 946.

(15) Wintgens, V.; Valat, P.; Kossanyi, J.; Demeter, A.; Biczok, L.; Berces, T. *J. Photochem. Photobiol., A* **1996**, *93*, 109.

(16) Miller, C. W.; Hoyle, C. E.; Valente, E. J.; Magers, D. H.; Jönsson, E.S. *J. Phys. Chem. A* **1999**, *103*, 6406.

(17) Matsuo, T. *Bull. Chem. Soc. Jpn.* **1965**, *38*, 557.

(18) Labhart, H.; Wagniere, G. *Helv. Chim. Acta* **1959**, *42*, 2219.

(19) Turro, N. J. *Modern Molecular Photochemistry*; University Science Books: Mill Valley, CA, 1991.

(20) Viswanathan, K.; Clark, S.; Miller, C.; Hoyle, C. E.; Jonsson, S.; Shao, L. *Polym. Prepr.* **1998**, *39* (2), 644.

(21) Horspool, W.; Armesto, D. *Organic Photochemistry: A Comprehensive Treatment*; Ellis Horwood Ltd.: New York, 1992.
(22) Grimshaw, J.; de Sliva, A. P. *Chem. Soc. Rev.* **1981**, *10*, 181.
(23) Bunce, N. J.; Bergsma, J. P.; Bergsma, M. D.; De Graaf, W.; Kumar, Y.; Ravanal, L. *J. Org. Chem.* **1980**, *45*, 3708.
(24) Scaiano, J. C.; Nicodem, D. E. *Can. J. Chem.* **1984**, *62*, 2346.
(25) Creed, D.; Hoyle, C. E.; Jordon, J. W.; Pandy, C. A.; Nagarajan, R.; Pankasem, S.; Peeler, A. M.; Subramanian, P. *Macromol. Symp.* **1997**, *116*, 1.
(26) Barlow, J. H.; Davison, R. S.; Lewis, A.; Russel, D. R. *J. Chem. Soc., Perkin Trans. 2* **1979**, 1103.
(27) Sonntag, J. V.; Knolle, W. *J. Photochem. Photobiol., A* **2000**, *136*, 133.